Establishing the relation between detrended fluctuation analysis and power spectral density analysis for stochastic processes

C. Heneghan[1] and G. McDarby[1,2]
[1]*Digital Signal Processing Research Group, University College Dublin, Belfield, Dublin 4, Ireland*
[2]*Biomedical Systems Laboratory Group, University of New South Wales, Sydney, NSW, Australia*
(Received 24 March 2000; revised manuscript received 24 July 2000)

Stochastic fractal signals can be characterized by the Hurst coefficient *H*, which is related to the exponents of various power-law statistics characteristic of these processes. Two techniques widely used to estimate *H* are spectral analysis and detrended fluctuation analysis (DFA). This paper examines the analytical link between these two measures and shows that they are related through an integral transform. Numerical simulations confirm this relationship for ideal synthesized fractal signals. Their performance as estimators of *H* is compared based on a mean square error criterion and found to be similar. DFA measures are derived for physiological signals of heartbeat *R-R* intervals through the integral transform of a spectral density estimate. These agree with directly calculated DFA estimates, indicating that the relationship holds for signals with nonideal fractal properties. It is concluded that DFA and spectral measures provide equivalent characterizations of stochastic signals with long-term correlation.

PACS number(s): 05.40.−a, 05.45.Tp, 87.10.+e

I. INTRODUCTION

Stochastic fractal signals arc characterized by a variety of unusual statistical properties, such as self-similarity (or self-affinity), power-law statistics, and correlation over all scales. These signals are of interest since they can be used to model phenomena as diverse as heart-rate variability [1–7], the sequence of base pairs in DNA [8,9], financial volatility [10–12], gait fluctuation [13], image texture [14], and cloud breaking [15]. They can be characterized in a number of ways—by their fractal dimension *D*, through the Hurst coefficient *H*, or by estimating a scaling exponent α of their power-law statistics. One motivation for estimating *D*, *H*, or α lies in the fact that these measures may potentially be used to classify or discriminate between different types of signal, e.g., Amaral *et al.* have suggested that a scaling exponent may distinguish between healthy and pathological heart dynamics [5]. In order for such classification schemes to be robust, estimates of the fractal dimension must be accurate and reliable, and hence much interest has centered on suitable approaches for estimating the fractal dimension, or related parameters, from experimental data sets. Techniques that have been proposed for the estimation of fractal behavior include correlograms and semivariograms [16], spectral analysis [17], rescaled range analysis [18], the Fano factor [19], Allan variance [20], wavelet transform variance [21,22], detrended fluctuation analysis [9], scaled windowed variance analysis [23], dispersional analysis [24], and maximum likelihood estimators [14,25]. Two good review articles of the range of techniques available are the papers by Malamud and Turcotte [16] and by Taqqu, Teverovsky, and Willinger [25]. These articles, and others [17,26], report on comparative empirical studies of these techniques and the performance of the various estimators. The theoretical relationship between some of these techniques has also been explored. For instance, the relationship between dispersional analysis and the correlation function of the underlying process is established in [23], and that between spectral analysis and fractal dimension was shown in [27]. In this vein, one of the present authors (and others) attempted to provide further linkage between the different techniques available. In [28], explicit links were forged between wavelet variance estimation, Allan variance, the Fano factor, and power spectral density (PSD), and it was shown that all these measures could be expressed in terms of the power spectral density of the signal.

Of the measures outlined above, detrended fluctuation analysis (DFA) has recently been widely adopted in the physical and biological sciences. Some of these reports imply that the DFA measure provides information that could not have been otherwise obtained, or that it is inherently a superior measure to existing techniques. For example, in [7], both spectral and DFA measures are used to assess changes in neuroanatomic function, with the implication that these measures were providing distinct views of the data. Indeed, in the original paper introducing DFA, the authors proposed it as an *independent* measure of long-term correlation, complementary to spectral analysis [9]. To our knowledge, however, the link between DFA and existing measures has not been clearly elucidated. It is the goal of this paper to show that DFA is simply related to the power spectral density (and indeed can be derived directly from a spectral density estimate), and hence to other measures such as wavelet variance. Allan variance, and the Fano factor. The motivation for this is to clearly demonstrate that DFA does not provide any information that cannot be obtained through spectral analysis. We present numerical simulations of ideal fractal signals in which a direct DFA calculation (by least-squares detrending) and a derived DFA measure (calculated from the integration of a PSD estimate) are shown to provide equivalent results. In addition, we provide some comparison of the performance of the DFA measure and spectral density techniques in estimating *H* for ideal fractal signals, and show

that their performance is similar. To confirm that the equivalence holds for signals that have a combination of fractal and nonfractal behavior, we calculate direct and derived DFA measures for heart-rate signals. As further confirmation, the DFA measure at a specific scale is shown to provide statistical discrimination between normal and pathological data sets, as previously shown using a spectral measure only [28].

Fractional Brownian motion and fractional gaussian noise

Two classes of signal have been widely used to model stochastic fractal time series: fractional Gaussian noise (FGN) and fractional Brownian motion (FBM). These are, respectively, generalizations of white Gaussian noise and Brownian motion. They are related by the fact that increments of a FBM form a FGN process (or alternatively FBM represents cumulative summation or integration of a FGN). A formal mathematical definition of continuous FBM was first offered by Mandelbrot and Van Ness [29]. To summarize, a FBM $b(t)$ is characterized by having Gaussian amplitude statistics and an autocorrelation function of the form

$$\mathrm{cov}[b(t_1)b(t_2)] = k_1(|t_1|^{2H} + |t_2|^{2H} - |t_1 - t_2|^{2H}), \quad (1)$$

where k_1 is a constant, and the parameter H varies between 0 and 1. H is usually referred to as the Hurst parameter as it can be traced to the parameter used by Hurst in his fundamental studies in the field [18]. Since this autocorrelation function is not a function of $t_1 - t_2$, the power spectral density of FBM is not well defined. However, by appealing to generalized concepts such as the Wigner-Ville spectrum [30], a limiting power spectrum can be obtained as follows:

$$S_b(f) = \frac{k}{|f|^{\alpha}}, \quad (2)$$

where $\alpha = 2H + 1$. The scaling exponent α of this power-law spectrum lies between 1 and 3, since H is constrained to lie between 0 and 1.

The autocorrelation function for fractional Gaussian noise can be obtained by defining a process $g(t)$ as the increments of a corresponding FBM $b(t)$, to yield

$$\mathrm{cov}[g(t_1)g(t_2)] = k_2(|t_2 - t_1|^{2H}), \quad (3)$$

where k_1 is a constant, and H is the Hurst parameter as before. The Fourier transform of this autocorrelation function is also not well defined, but as for FBM a limiting power spectrum can be found as follows:

$$S_g(g) = \frac{k}{|f|^{\alpha}} \quad (4)$$

where $\alpha = 2H - 1$. Since H lies between 0 and 1, the scaling exponent α of the power-law spectrum of FGN lies between -1 and 1. Therefore the complete set of FGN and FBM stochastic sequences are defined to have power-law spectra with exponents lying between -1 and 3. Further fractal processes could be defined with PSD power-law exponents outside this range, but in this paper we will restrict our attention to FGN and FBM as defined above.

Discrete versions of FBM and FGN (DFBM and DFGN, respectively) can also be formed [14]. Some care is needed in their definition, since theoretically the continuous FBM and FGN have infinite bandwidth. Hence the process of sampling will introduce some aliasing. This is particularly significant for DFGN since the high frequency components are of higher magnitude than for DFBM. In this paper, we will define DFBM as samples of a continuous FBM, with a sampling rate T_s,

$$b[n] = b(t)|_{t = nT_s}, \quad (5)$$

and take the aliasing effects as negligible. DFGN will then be defined as the first differences of the DFBM:

$$g[n] = b[n] - b[n-1]. \quad (6)$$

Following on from these definitions, the autocovariance and autocorrelation functions of DFBM and DFGN can be written as

$$E[b[j]b[k]] = k_2(|j|^{2H} + |k|^{2H} - |j-k|^{2H}), \quad (7)$$

$$E[g[n+k]g[n]] = r_{gg}[k] = \frac{\sigma^2}{2}[|k+1|^{2H} - 2|k|^{2H} + |k-1|^{2H}], \quad (8)$$

where k_2 is a constant, and σ^2 is the variance of $x[n]$. Since most real data sets are measured samples of some underlying continuous process, it seems reasonable to use the DFBM and DFGN models throughout this paper.

As clearly noted in [31], some of the estimators of H have a built-in assumption as to whether the signal under analysis is FGN or FBM, and will provide incorrect estimates of H if the signal model is incorrect. This point is often overlooked or ignored by many researchers. For example, dispersional analysis is appropriate only for FGN, whereas scaled windowed variance is better for FBM [23]. Some methods (such as spectral analysis and DFA) can be used for both FGN and FBM processes.

For completeness we mention that the Hurst parameter H is related to the Hausdorff-Besicovich dimension D through $H = 2 - D$ [32]. D is the parameter most generally defined as the ''fractal dimension,'' and lies between 1 and 2 for FGN and FBM.

II. THEORY

Many different techniques for estimating H from experimental data sets have been proposed. This paper focuses on estimating H using power spectral density estimation and detrended fluctuation analysis, and on how these estimates are related.

A. Detrended fluctuation analysis

Detrended fluctuation analysis was originally proposed as a technique for quantifying the nature of long-range correlations by Peng *et al.* in 1994 [8]. It was introduced in order to permit the detection and quantification of long-range correlations in DNA sequences. As implied by its name, it was conceived as a method for detrending local variability in a sequence of events, and hence providing insight into long-

term variations in the data sets. This technique has subsequently been used in the analysis of heart-rate variability [1–16], gait behavior [13], financial volatility [10–12], meteorology [15], and geology [16]. Different authors have used slightly alternative terminology to describe this technique. In [31], DFA is cast as a special case of scaled windowed variance referred to as ''linear regression detrended scaled windowed variance,'' and Taqqu, Teverovsky, and Willinger refer to it as the ''residuals of regression'' [25].

The DFA algorithm consists of the following steps.

(i) The data to be analyzed are a discrete-index sequence $u[n]$ defined for $0 \leqslant n \leqslant L-1$. It can be assumed that the sampling rate for this sequence is unity without loss of generalization. The average value of this sequence is set to zero, by subtracting the sample mean. A running summation sequence $y[n]$ is constructed from this sequence using the following recursion:

$$y[n]=\sum_{k=0}^{n-1} u[k], \quad y[0]\equiv 0, \quad y[n]\equiv 0 \quad \forall n<0, \tag{9}$$

which can be recognized as the output of a simple infinite impulse response (IIR) filter applied to $u[n]$:

$$H(z)=\left\langle \frac{Y(z)}{U(z)} \right\rangle = \frac{1}{1-z^{-1}}. \tag{10}$$

(ii) The entire sequence is divided into M nonoverlapping blocks $y_m[n]$, each containing K samples (so that $M=L/K$):

$$y_m[n]=y[mK+n], \quad 0 \leqslant m \leqslant M-1, \quad 0 \leqslant n \leqslant K-1. \tag{11}$$

The local ''trend'' in each block is defined to be a linear least-squares fit to the samples in that block. The trend is denoted as $y_{m,t}[n]$.

(iii) A detrended signal is defined for each block as the difference between the original signal and the local trend for that block, leading to

$$y_{m,d}[n]=y_{m,t}[n]-y_m[n], \quad 0 \leqslant m \leqslant M-1, \quad 0 \leqslant n \leqslant K-1 \tag{12}$$

The variance of the detrended signal is calculated for each block. $F_1(K)$ is then defined as the average of the variances over all boxes:

$$F_1(K)=\frac{1}{M}\sum_{m=0}^{M-1} \mathrm{var}(y_{m,d}[n]). \tag{13}$$

The functional dependence of $F_1(K)$ is obtained by evaluations over all block sizes K. It has been shown by Buldyrev *et al.* that $F_1(K)$ varies as a power law in K, i.e., $F_1(K) \approx K^{\beta}$ for sequences with power-law long-range correlations such as FBM and FGN [9]. An alternative derivation of this relationship is given in [25]. The parameter β can therefore be used to estimate H, since it has been empirically determined that $\beta-1=\alpha$, the spectral power-law exponent, which in turn can be related to H [9]. An estimate of β can be calculated from $F_1(K)$ by a linear least-squares fit to a log-log plot of K vs $F_1(K)$.

B. Spectral analysis

Spectral analysis using nonparametric estimation techniques such as averaged windowed periodograms (Welch's algorithm) is a long-established technique for estimating the parameters of fractal behavior. Power-law exponents α can be calculated from the spectral density estimate by fitting a linear least-squares fit to a log-log plot of frequency vs spectral density estimate. The relationship between the spectral exponent α and H is known to be $\alpha=2H-1$ for FGN and $\alpha=2H+1$ for FBM. Therefore, the relation between spectral and DFA power-law exponents (α and β, respectively) is simply given by $\alpha=\beta-1$. However, the exact relation between DFA and power spectral density spectral analysis has not yet been elucidated.

C. Relation between detrended fluctuation analysis and spectral analysis

This well-known relation between the two power-law exponents suggests that a direct analytical link can be found between the two measures. To explore this link, consider the various steps used in defining the DFA measure.

The DFA of the sequence $u[n]$ is found according to the algorithm described above. Let us denote the power spectral density of the discrete sequence as $S_u(\omega)$. The first step in the algorithm subtracts the sample mean from $u[n]$ resulting in a new sequence $u_0[n]$ that has zero mean. This new process has a power spectral density everywhere equal to $S_u(\omega)$, except at $\omega=0$ where it assumes a value of zero. The summation of this zero-mean sequence generates the series $y[n]$, as shown in Eq. (3). This new sequence has a power spectral density given by

$$\begin{aligned} S_y(\omega) &= |H(e^{j\omega})|^2 S_{u_0}(\omega) \\ &= \begin{cases} 0, & \omega=0 \\ \dfrac{S_u(\omega)}{2(1-\cos\omega)} \approx \dfrac{S_u(\omega)}{\omega^2} & \text{for small } \omega, \quad \omega \neq 0. \end{cases} \end{aligned} \tag{14}$$

The sequence $y[n]$ is then divided into segments of length K, resulting in M segments $y_m[n]$ for $m=0,1,\ldots,M-1$, before detrending to produce the signal $y_{m,d}[n]$.

Several observations can be made about the set of signals $y_{m,d}[n]$. First, these are zero-mean signals since by definition a least-squares fit will produce a zero-mean residual. The signals will be mutually uncorrelated at scales greater than K, since variations on time scales longer than K have been removed. Moreover, the linear fit coefficients are chosen so that the residual has a minimum variance (by definition of least squares). The variance of a signal is equal to the area under its power spectral density; therefore minimizing the variance requires generating a detrended signal whose power spectral density has the least area possible. Since the subtracted signals $y_{m,t}[n]$ have the bulk of their power at frequencies below $1/K$, the best way to minimize the variance of the detrended signals is to set their power spectral density to zero over the range $0-1/K$. It is easy to verify numerically that the power spectral densities of detrended signals obey the following relation quite closely:

$$S_{y_{m,d}}(\omega) \approx \begin{cases} 0, & 0 \leqslant \omega \leqslant \pi/K \\ S_{y_m}(\omega) & \text{otherwise.} \end{cases} \tag{15}$$

A complete detrended signal $y_d[n]$ is constructed by piecing back the individual segments. The overall signal will have the property that it has negligible power at frequencies below π/K. This signal will have a zero sample mean since each individual segment has a sample zero mean. The variance of the detrended signal is then calculated for each box, and an estimate of $F_1(K)$ is defined as the average of the variances over all boxes:

$$\hat{F}_1[K] = \frac{1}{M} \sum_{m=0}^{M-1} \hat{\text{var}}(y_{m,d}[n]) \tag{16}$$

where the caret denotes a statistical estimate. In fact, it is easily shown that the sum of variances equals the variance of the complete signal $y_d[n]$ in this particular case. To do so, assume a simple variance estimator such as

$$\begin{aligned} \hat{\text{var}}(y_d[n]) &= \frac{1}{L} \sum_{n=0}^{L-1} (y_d[n] - \overline{y_d}[n])^2 \\ &= \frac{1}{L} \sum_{n=0}^{L-1} (y_d[n])^2, \end{aligned} \tag{17}$$

where the overbar denotes a sample average, and the final term on the right-hand side (RHS) derives from the fact that the sample mean of the overall detrended signal is 0. Equation (17) can be rewritten as

$$\begin{aligned} \hat{\text{var}}(y_d[n]) &= \frac{1}{L} \sum_{n=0}^{L-1} (y_d[n])^2 \\ &= \frac{1}{MK} \sum_{m=0}^{M-1} \sum_{n=0}^{K-1} (y_{m,d}[n])^2 \\ &= \frac{1}{M} \sum_{m=0}^{M-1} \left(\sum_{n=0}^{K-1} (y_{m,d}[n] - \overline{y}_{m,d}[n])^2 \right) \end{aligned} \tag{18}$$

since $\overline{y}_{m,d}[n] = 0$ for each segment. The final term on the RHS of Eq. (18) can therefore be recognized as $\hat{\text{var}}(y_{m,d}[n])$, which yields the equivalence between Eq. (17) and Eq. (18).

However, the variance of the signal $y_d[n]$ can also be calculated by integrating its power spectral density. Assuming a window size of K, this yields

$$\begin{aligned} F_2[K] &= \hat{\text{var}}(\nu_d[n]) \\ &= \int_{\omega=0}^{\pi} S_{y_d}(\omega) d\omega \\ &= \int_{\omega=1/K}^{\pi} \frac{S_u(\omega)}{2(1-\cos\omega)} d\omega, \end{aligned} \tag{19}$$

where we have used Eq. (15). If our reasoning is correct, then $F_2(K) = F_1(K)$. By considering the continuous-time analog of this approach, we can easily check for the observed relation between α and β. Assume the case of a continuous-time FGN or FBM with a known power-law power spectral density,

$$S_u(\omega) = \frac{c}{\omega^\alpha}, \tag{20}$$

where c is an arbitrary constant. In the continuous case, summation is replaced by integration, which has the effect of dividing the power spectral density by ω^2. Therefore, following the same reasoning as for the discrete signal case, we obtain

$$\begin{aligned} F_2[K] &= \int_{\omega=1/K}^{\omega} \frac{c}{\omega^2 \omega^\alpha} d\omega \\ &= \frac{-c}{1+\alpha} \omega^{-(1+\alpha)} \Big|_{\omega=1/K}^{\omega=\infty} \\ &= \frac{-c}{1+\alpha} K^{1+\alpha} \propto K^\beta, \end{aligned} \tag{21}$$

where $\beta = \alpha + 1$ as experimentally observed.

D. Discrete formulation

A discrete formulation of Eq. (19) can be used to form an estimate of the DFA directly from a power spectral density estimate. The discrete formulation is formed in the following way. A power spectral density of the original sequence $u[n]$ is estimated using a standard nonparametric technique such as Welch's algorithm. This leads to a set of discrete samples of the estimated power spectral density denoted as $S[k] = S_u(k\Delta\omega)$ for $0 \leqslant k \leqslant N/2$, where $\Delta\omega$ is the frequency spacing $2\pi/N$, and N is the number of points used in forming the individual periodograms that form the power spectral density estimate. The value of $S(\omega)$ at $\omega = \pi/K$ can be estimated by linear interpolation of its value at the integers closest to $\omega = \pi/K$. Defining L^+ as the first integer greater than π/K and L^- as $L^+ - 1$, the discrete approximation of Eq. (19) becomes

$$\begin{aligned} F_2[K] = \Delta\omega \sum_{k=L^+}^{N/2} \frac{S[k]}{2(1-\cos 2\pi k/N)} &+ \left(\frac{\pi}{K} - L^- \right) S[L^-] \\ &+ \left(L^+ - \frac{\pi}{K} \right) S[L^+]. \end{aligned} \tag{22}$$

This formulation provides an explicit formula therefore for evaluating the DFA simply from a power spectral density estimate. In this paper, we will term such a value a *derived* DFA calculation (since it is derived from the PSD estimate). By examining the variation of $F_2(K)$ as a function of K, a power-law exponent γ can be derived from this discrete approximation, which should be equal to β obtained by direct calculation of DFA. The numerical simulations presented

here confirm the high level of agreement between the values of β and γ obtained using both derived and direct calculation of DFA. The numerical simulations presented here confirm the high level of agreement between the values of β and γ obtained using both derived and direct calculation of DFA.

III. RESULTS

A. Synthesized sequences with long-term correlation

Data sequences of length $L=32\,768$ representing discrete-time samples of FGN and FBM were generated using the spectral synthesis method. This works by generating a signal from a periodogram that has a power-law fall-off. Discrete-frequency samples $G[k]$ were generated that decreased in a power-law fashion with frequency index k, i.e.,

$$G[k]=\begin{cases} G_0, & k=0 \\ \dfrac{G_0}{k^a}, & 1\leqslant k<L/2 \\ \dfrac{G_0}{(L/2)^a}, & k=L/2 \\ G^*[k], & L/2<k\leqslant L. \end{cases} \tag{23}$$

The $G[k]$ are given random uniformly distributed phases, and complex conjugate symmetry is preserved. For $0<\alpha<1$, the inverse discrete Fourier transform of the sequence $G[k]$ yields a real-valued discrete-index sequence representing samples of FGN. Discrete FBM is generated using summation of the FGN sequences. Alternative synthesis techniques (such as that proposed by Davies and Harte [33]) were also evaluated, and gave similar results in terms of the relationship between spectral analysis and DFA.

To verify the relations discussed previously, the direct DFA algorithm was applied to control sequences generated in this fashion. $F_1(K)$ was evaluated at octave-spaced values of K, i.e., 16,32 , . . . , etc. In order to provide reasonable estimates of $F_1(K)$, the largest window size used was $L/32=1024$. Following calculation of the DFA, a plot was formed of K vs $F_1(K)$. The power-law exponent was estimated by a least-squares linear fit to the curve on a log-log scale. The full range of K values was used in fitting this curve. The slope of the resulting best fit line was then used as the estimate of the DFA power-law exponent $\hat{\beta}$.

To confirm the hypothesis that the DFA power-law exponent can also be calculated via an estimate of the power spectral density of a signal using Eq. (22), we calculated a power-law exponent $\hat{\gamma}$ by a linear least-squares fit to the plot of $F_2(K)$ vs K. To do this, power spectral density estimates of the same sets of data were formed using the Welch algorithm with rectangular nonoverlapping windows of length $L/2$. These PSD estimates were used in the summation of Eq. (22).

Figure 1 shows the results of these simulations by plotting the values of $\hat{\beta}$ against $\hat{\gamma}$. The values plotted were based on the mean exponents of 50 simulated sequences, with a range of values for H from 0.05 to 0.95. The range of β from 0 to 2 indicates the regime of FGN, while 2 to 4 corresponds to

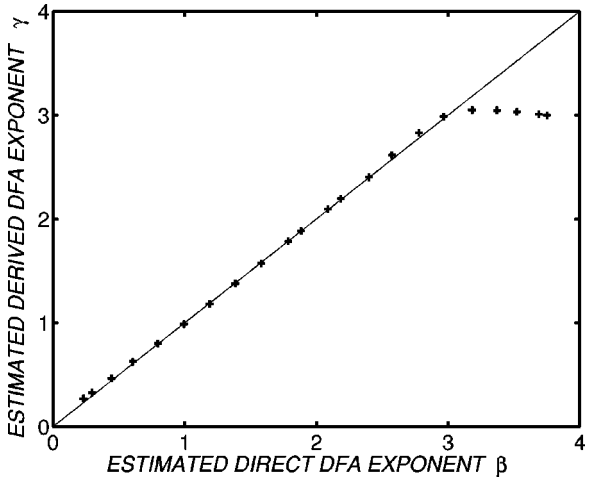

FIG. 1. A comparison of estimated power-law exponents from synthesized data sequences using direct detrended fluctuation analysis (β), and derived detrended fluctuation analysis (γ). The line indicates ideal agreement between the two estimators, i.e., $\beta=\gamma$. The values of H used in the synthesis routines varied from 0 to 1, and both FGN and FBM sequences were simulated. Fifty sequences of length $L=32\,768$ were generated for each value of H. The plus symbols indicate the mean values of the calculated exponents. β was calculated by evaluating $F_1(K)$ at octave-spaced values of K from 32 to 2048. γ was derived from $F_2(K)$ based on power spectral densities using Welch's method (with a rectangular window of 16 384 samples), and the same range of K values as for β. The value of $\beta,\gamma=2$ indicates the division between FGN and FBM processes.

FBM processes. For FGN, the agreement between direct and derived DFA exponents is excellent. For FBM processes, the agreement is also excellent up to the value $\gamma=3$. At this value the derived DFA exponent saturates. This saturation is due to a windowing effect in the calculation of the PSD estimate. Numerical simulation with a Bartlett window in place of a rectangular window has shown that the exponent at which saturation occurs is dependent on the fall-off of the window's aperiodic autocorrelation near $\omega=0$. This windowing effect also limits the use of the rectangular window in spectral density analysis for FBM where $H>0.5$. This effect was first noted by Fougere in [34]. As a side note, if FSD estimation based on Welch's algorithm with a rectangular window yields an estimated H of close to 0.5 for a FBM, a more suitable window such as the Bartlett or Hanning window should be applied in the spectral analysis.

We are also interested in the bias and variance of the DFA measures when used to estimate H. Figure 2 shows numerical results that indicate the bias and variance of both estimators, by showing the mean estimated value of H and its standard deviation for the synthesized signals. Since the observed estimated H values obey approximately Gaussian statistics, the standard deviation is a reasonable measure of error. The left-hand column of panels shows the estimated H for FGN when direct (upper panel) and derived (lower panel) DFA exponents are used. They share similar biases, and the variance of the derived DFA estimator is slightly lower than that for the direct DFA. Both show quite a large bias near $H=0$. The right panel shows estimates of H for FBM using $F_1(K)$ and $F_2(K)$. In this case, both estimators display sig-

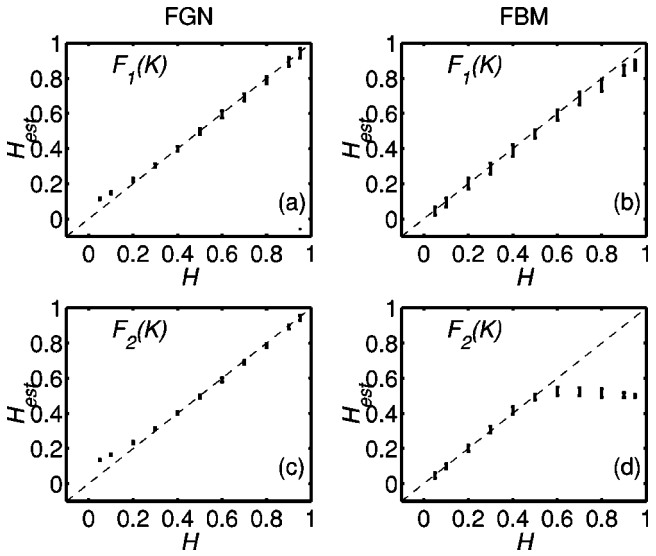

FIG. 2. A comparison of the estimated Hurst parameters H using both direct detrended fluctuation analysis (β), and derived detrended fluctuation analysis (γ). For FGN, the ideal behavior is given by $\beta,\gamma=2H$. For FBM, the expected behavior is $\beta,\gamma=2H+2$. The line indicates ideal agreement between the value of H fed into the simulations and the calculated H_{est} based on β and γ. The values of H used in the synthesis routines varied from 0 to 1, and both FGN and FBM sequences were simulated. Fifty sequences of length $L=32\,768$ were generated for each value of H. The error bars indicate the standard deviations on the estimated values of H. (a) shows the estimated H using $F_1(K)$ for FGN processes. (b) shows the estimated H using $F_1(K)$ for FBM processes. (c) shows the estimated H using $F_2(K)$ for FGN processes. (d) shows the estimated H using $F_2(K)$ for FBM processes. The saturation in the estimate of H observed in (d) is explained in the text.

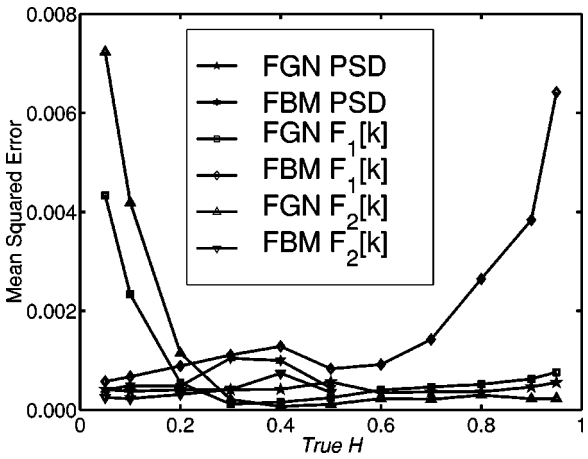

FIG. 3. A comparison of the performance of PSD, direct DFA, and derived DFA estimators for H. The mean squared error for each estimator was calculated based on 50 sequences of length $L=32\,768$ for various values of H between 0 and 1. The MSE's for the PSD and derived DFA estimators of $H>0.5$ for FBM are not included, as they have a known strong bias.

nificant bias for $H>0.5$. As noted in Fig. 1, the derived DFA exponent will saturate at a value of $\beta=3$ which corresponds to $H=0.5$ for FBM. As before, use of a nonrectangular window will remove this bias. As noted for FGN, the derived DFA exponent has slightly lower variance.

A general rule for statistical estimators of the sort discussed here is that there is a trade-off between the bias and variance of the estimator. In this case it is possible to decrease the variance of our estimators by taking the linear regression (from which the power-law exponent is extracted) over a larger range of values. However, lowering the variance in this manner, will occur at the expense of increasing bias. This effect was also noted in [31], where the authors have attempted to provide guidelines for the optimum choice to minimize the bias-variance product. Since both bias and variance contribute to the overall performance, a suitable technique for providing a global measure of performance is to use the mean square error (MSE), which combines the confounding effects of both bias and variance [31,25]. This evaluates the average square error for the estimate of H. The error is defined as the difference between the H fed to the synthesis routine and the estimated H. Its value will be influenced not only by the estimator of H, but also by the synthesis technique used. However, since all estimators are using the same synthesized sequences, this effect should be constant across all three. Figure 3 shows the MSE defined for three estimates of H (calculated from direct DFA, derived DFA, and PSD analysis), for both FGN and FBM signals. The MSE for the derived DFA and the PSD for FBM with $H>0.5$ is not shown as it has a large bias whose cause is known. This graph shows several points of interest. First, neither the derived nor the direct DFA perform consistently better than each other. For example, the derived DFA is worse than the direct DFA estimator for FGN with $H<0.5$, but better for FBM with $H>0.5$. Secondly, the MSE of the PSD estimator is more consistent across the range of H, and is never significantly worse than either of the DFA estimators. This result confirms that use of the DFA should not be preferred over spectral analysis, and that in general quite similar performance can be expected for both types of estimator. Interested readers can compare our results with Fig. 11 of [31], which shows nearly identical behavior of the MSE of the DFA estimator as a function of H.

B. Application to physiological data

The results of Figs. 1 and 2 confirm that the two techniques for calculating DFA provide equivalent results, for the case of signals with exact known long-term correlations which can be characterized by a single power-law exponent. However, the link between PSD and DFA measures is not dependent upon the signal conforming to the model of a simple FGN or FBM. To confirm this, we will apply the direct DFA and derived DFA measures to a set of data characterizing heart-rate variability. These data sets record the interbeat intervals (R-R) between heartbeats recorded using a Holter monitor. These data sets form part of the Massachusetts Institute of Technology–Beth Israel Hospital (MIT-BIH) heart-failure database. They comprise 12 records from normal patients and 15 records from heart-failure patients. These data sets can be modeled as a combination of a fractal stochastic process and a collection of frequency specific stochastic processes (with time scales set by breathing and other mechanisms). Figure 4(a) shows a comparison of the DFA

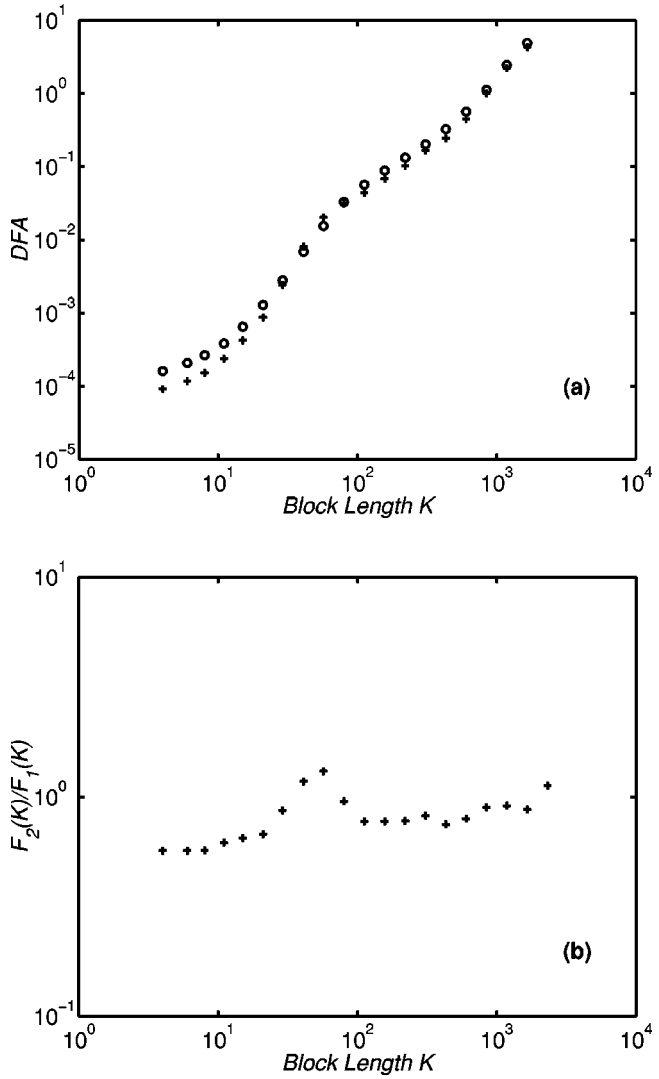

FIG. 4. (a) A comparison of $F_1(K)$ and $F_2(K)$ calculated for a data set from the Beth-Israel heart database (record number a7257.asc). This record contains 118 376 *R-R* intervals. The circles correspond to $F_1(K)$ and the plus symbols correspond to $F_2(K)$. (b) The ratio of $F_2(K)/F_1(K)$ as a function of *K*.

calculated using both the direct and derived methods. The two curves agree closely. To verify that the slight error between them is not biased, Fig. 4(b) shows the ratio of $F_2(K)/F_1(K)$ as a function of *K*. The difference between the two can probably be attributed to the process of numerical integration and deviations between the estimated PSD and the true PSD of the process.

In previous work, we used power spectral density estimates to provide a characteristic frequency region that statistically separated normal and abnormal subjects [35]. Since our analysis shows that DFA is directly related to PSD, it should also be possible to provide a region of separability using either the direct or derived DFA measures. Figure 5 gives the results of calculating $F_2(K)$ for this set of data. The dotted curves indicate the normal data sets, and the solid curves are abnormal sets. Within the region *S* delineated by the values $K=16$ and $K=40$, all of the normal data sets have higher values of $F_2(K)$ than abnormal data sets. This suggests that the dynamics of heart-rate variability are different

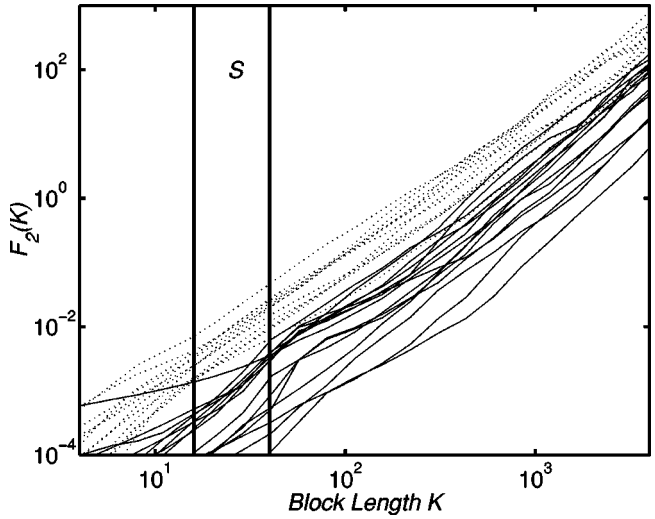

FIG. 5. Evaluation of $F_2(K)$ (the derived DFA measure) for all 27 data sets in the Beth-Israel *R-R* interval database. The dotted curves are calculated from normal data sets, and the solid curves are from abnormal data sets. For the values of *K* from 16 to 40 (denoted by *S* in this plot), $F_2(K)$ provides complete separation between the two classes of data set, suggesting that the dynamics of heart-rate variability differ significantly for normal and pathological hearts over a time scale corresponding to 16–40 beats.

for abnormal and normal subjects over time scales corresponding to 16–40 beats. This is consistent with our estimate of a characteristic region of 16–32 beats based on PSD analysis. It also confirms that the equivalence of DFA and PSD based measures holds for real-world signals that combine long-term correlation and scale-specific effects.

As a final note, we should mention the difference in computational complexity between the direct and derived DFA measures. The direct DFA can be shown to be an $O(n^2)$ computation, whereas the derived DFA, which is built on a spectral density estimate, is only of order $O(n \log n)$. As a consequence, there is a significant difference in computational requirements between the two methods (refer to Table 2 of [28]).

IV. CONCLUSIONS

We have demonstrated analytically that detrended fluctuation analysis can be related to the underlying power spectral density of the stochastic data. This analytical work is confirmed by numerical simulations, and by the analysis of real physiological signals extracted from the MIT-BIH electrocardiogram database. The performance of spectral and DFA measures has been compared using a mean square error criterion, and found to be comparable. *We conclude therefore that DFA and spectral analysis will yield highly similar values of H, and should not be treated as independent measures of the long-term properties of a stochastic signal.* This explains the effect noted in [9] in which the authors note that ''the values of β and of $\beta' \equiv 2\alpha - 1$ are remarkably close to each other'' (where β represents the DFA exponent and α is the PSD exponent). Our results are also consistent with their observation that the standard deviation of the direct DFA exponent was lower than for the spectral based measure. This

can be explained by the bias-variance trade-off. Their report explicitly notes a consistent bias between the spectral and DFA estimates. The derived DFA measure is also computationally more attractive than the direct DFA, since it is an $O(n \log n)$ computation. We note as a caveat that the derived DFA measure can suffer from saturation effects if we are trying to estimate exponents from sequences with spectra of the form $1/|f|^{\alpha}$ with $\alpha \geqslant 2$, although by different choice of windows in PSD estimation the range of allowable processes can be extended. We conclude that there is no particular reason to recommend the use of detrended fluctuation analysis over spectral analysis for stochastic processes with long-term correlation.

ACKNOWLEDGMENTS

The authors are grateful to P. Curran, M. C. Teich, S. B. Lowen, B. Jost, and K. Vibe-Rheymer for useful discussion. This work was supported by Enterprise Ireland under International Collaboration Grant No. IC/98/018 (C. H.) and the Biomedical Systems Laboratory at University of New South Wales, Australia (G.McD.).

[1] M. Kobayashi and T. Musha, IEEE Trans. Biomed. Eng. **BME-29**, 456 (1982).
[2] C.-K. Peng, S. Havlin, H. E. Stanley, and A. L. Goldberger, Chaos **5**, 82 (1995).
[3] C.-K. Peng, S. Havlin, J. M. Hausdorff, J. Mietus, H. E. Stanley, and A. L. Goldberger, J. Electrocardiol. **28**, 59 (1996).
[4] M. Barbi, S. Chillemi, A. Di Garbo, Balocchi, C. Carpeggiani, M. Emdin, C. Michelassi, and E. Santarcangelo, Chaos, Solitons Fractals **9**, 507 (1998).
[5] L. A. Nunes Amaral, A. L. Goldberger, P. Ch. Ivanov, and H. E. Stanley, Phys. Rev. Lett. **81**, 2388 (1998).
[6] T. H. Makikallio, J. Koistinen, L. Jordaens, M. P. Tulppo, N. Wood, B. Golosarsky, C. K. Peng, A. L. Goldberger, and H. V. Huikuri, Am. J. Cardiol. **83**, 880 (1999).
[7] D. Toweill, K. Sonnenthal, B. Kimberley, S. Lai, and B. Goldstein, Crit. Care Med. **28**, 2051 (2000).
[8] C. K. Peng, S. V. Buldyrev, S. Havlin, M. Simons, H. Stanley, and A. L. Goldberger, Phys. Rev. E **49**, 1685 (1994).
[9] S. V. Buldyrev, A. L. Goldberger, S. Havlin, R. N. Mantegna, M. E. Matsa, C.-K. Peng, M. Simons, and H. E. Stanley, Phys. Rev. E **51**, 5084 (1995).
[10] Y. Liu, P. Cizeau, M. Meyer, C.-K. Peng, and H. E. Stanley, Physica A **245**, 437 (1997).
[11] N. Vandewalle and M. Ausloos, Physica A **246**, 454 (1997).
[12] N. Vandewalle and M. Ausloos, Phys. Rev. E **58**, 6832 (1998).
[13] J. M. Hausdorff, S. L. Mitchell, R. Firtion, C.-K. Peng, M. E. Cudkowicz, J. Y. Wei, and A. L. Goldberger, J. Appl. Physiol. **82**, 262 (1997).
[14] T. Lundahl, W. J. Ohley, S. M. Kay, and R. Siffert, IEEE Trans. Med. Imaging **MI-5**, 152 (1986).
[15] K. Ivanova and M. Ausloos, Physica A **274**, 349 (1999).
[16] B. D. Malamud and D. L. Turcotte, J. Stat. Plan. Infer. **80**, 173 (1999).
[17] J.-S. Leu and A. Papamarcou, IEEE Trans. Inf. Theory **41**, 233 (1995).
[18] H. E. Hurst, Trans. Am. Soc. Civ. Eng. **116**, 770 (1951).
[19] M. C. Teich, IEEE Trans. Biomed. Eng. **36**, 150 (1989).
[20] M. C. Teich, C. Heneghan, S. B. Lowen, and R. G. Turcott, in *Wavelets in Medicine and Biology*, edited by A. Aldroubi and M. Unser (CRC Press, Boca Raton, FL, 1996).
[21] S. Thurner, M. C. Feurstein, and M. C. Teich, Phys. Rev. Lett. **80**, 1544 (1998).
[22] P. Flandrin, IEEE Trans. Inf. Theory **35**, 197 (1989).
[23] G. M. Raymond and J. B. Bassingthwaighte, Physica A **265**, 85 (1999).
[24] J. B. Bassingthwaighte and G. M. Raymond, Ann. Biomed. Eng. **23**, 491 (1995).
[25] M. S. Taqqu, V. Teverovsky, and W. Willinger, Fractals **3**, 785 (1995).
[26] H. E. Schepers, J. H. G. M. van Beek, and J. B. Bassingthwaighte, IEEE Eng. Med. Biol. Mag. **11**, 57 (1992).
[27] M. V. Berry and Z. V. Lewis, Proc. R. Soc. London, Ser. A **370**, 459 (1980).
[28] M. C. Teich, S. B. Lowen, B. M. Jost, K. Vibe-Rheymer, and C. Heneghan, in *Nonlinear Biomedical Signal Processing Vol. II: Dynamic Analysis and Modeling*, edited by M. Akay (IEEE Press, Piscataway, NJ, 2000).
[29] B. B. Mandelbrot and J. W. Van Ness, SIAM Rev. **10**, 422 (1968).
[30] W. Martin and P. Flandrin, IEEE Trans. Acoust., Speech, Signal Process. **ASSP-33**, 1461 (1985).
[31] M. J. Cannon, D. P. Percival, D. C. Caccia, G. M. Raymond, and J. B. Bassingthwaighte, Physica A **241**, 606 (1997).
[32] S. B. Lowen and M. C. Teich, Fractals **3**, 183 (1995).
[33] R. B. Davies and D. S. Harte, Biometrika **74**, 95 (1987).
[34] P. F. Fougere, J. Geophys. Res. B **90**, 4355 (1985).
[35] C. Heneghan, S. B. Lowen, and M. C. Teich, *Proceedings of the IEEE International Conference on Acoustics, Speech, and Signal Processing (ICASSP)* (IEEE Press, Piscataway, NJ, 1999), Vol. 3, p. 1393.